

AC susceptibility of an assembly of nanomagnets: combined effects of surface anisotropy and dipolar interactions

F. Vernay,^{*} and Z. Sabsabi, and H. Kachkachi[†]

*Laboratoire PROMES-CNRS (UPR-8521) & Université de Perpignan Via Domitia,
Rambla de la thermodynamique, Tecnosud, 66100 Perpignan, FRANCE.*

(Dated: February 29, 2024)

We compute the AC susceptibility of a weakly dipolar-interacting monodisperse assembly of magnetic nanoclusters with oriented anisotropy. For this purpose we first compute the relaxation rate in a longitudinal magnetic field of a single nanomagnet taking account of both dipolar interactions in the case of dilute assemblies and surface anisotropy. We then study the behavior of the real and imaginary components of the AC susceptibility as functions of temperature, frequency, surface anisotropy and inter-particle interactions. We find that the surface anisotropy induces an upward shift of the temperature at the maximum of the AC susceptibility components and that its effects may be tuned so as to screen out the effects of interactions. The phenomenological Vogel-Fulcher law for the effect of dipolar interaction on the relaxation rate is revisited within our formalism and a semi-analytical expression is given for the effective temperature is given in terms of *inter alia* the applied field, surface anisotropy and dipolar interaction.

I. INTRODUCTION

The dynamics of magnetic systems in the form of nanoclusters (nanoparticles or nanomagnets) assemblies is a rather challenging issue from the standpoint of fundamental physics as it requires a simultaneous investigation of both long-range inter-cluster interactions and the intricacies of inhomogeneous magnetism taking place inside the clusters. Even for the equilibrium properties, the problem is of a tremendous difficulty especially if one tries to take account of the internal structure of the cluster by regarding it as a many spin system. In fact, only advanced numerical approaches may offer a way out, though with a limited success inasmuch as one considers the effect of surface anisotropy and its interplay with the inter-cluster dipolar interactions. Recently, this issue has been tackled^{1,2} to some extent by representing each nanocluster by an effective macroscopic model³⁻⁶ with an energy potential whose coefficients are functions of the cluster's characteristics (size, shape, lattice crystal, spin-spin interactions). It was shown that the magnetic properties of an assembly may be improved by a tailored variation of the assembly parameters, such as its concentration and geometry, and the clusters intrinsic characteristics such as the size and shape. In this work, we investigate the joint effect of inter-cluster interactions and surface anisotropy on the dynamic behavior of the assembly, in the case of low concentration and not too strong surface effects. For this we study the AC susceptibility with a variable measuring frequency.

AC susceptibility of an assembly of magnetic nanoclusters has been studied by many authors during the last decades, experimentalists and theorists, by varying the applied magnetic field, temperature and frequency.⁷⁻²³ These studies have greatly contributed to improve our understanding of the superparamagnetic behavior of such systems and to provide estimates of their physical parameters. In particular, the size study²² of AC susceptibility, together with Mössbauer spectroscopy, of diluted

and concentrated assemblies of maghemite nanoclusters dispersed in polymer, has revealed the important role of surface effects. On the theoretical side, it is the first time that the joint effects of inter-cluster interactions and surface anisotropy on the AC susceptibility are considered in a single study.

According to Debye's model applied to assemblies of magnetic nanoclusters,⁷ the AC susceptibility is given by $\chi(\omega) = \chi_{eq} / (1 + i\omega\Gamma^{-1})$, where χ_{eq} is the static or equilibrium susceptibility, ω the frequency and Γ the clusters relaxation rate (inverse of relaxation time). This model describes the absorption by a single mode of the electromagnetic energy provided by the applied field. The dynamics of this mode is rather slow and characterized by the longitudinal relaxation time $\tau = \Gamma^{-1}$ corresponding to the population inversion from the blocked state to the superparamagnetic state. This transition corresponds on average to the crossing by each cluster's magnetic moment of its energy barrier. Therefore, in order to compute the AC susceptibility, one has to compute the longitudinal relaxation rate of a nanocluster in the assembly (described by an effective model) in a magnetic field.

The paper is organized as follows: Section II is devoted to the presentation of the model and the statement of the problem. This Section closes with a brief summary of the results for the equilibrium susceptibility obtained in Ref. 2 as a function of the applied field, temperature, surface anisotropy and including the contribution of long-range dipolar interaction. The formulas for the AC susceptibility are then derived in Section III: we first describe in details the evaluation of single nanocluster's relaxation rate Γ with both a uniaxial and a cubic anisotropy representing the surface effects; by using Debye's model the semi-analytical form of the AC susceptibility is then given at the end of the Section. In Section IV we deal with the main focus of the present work, namely the study of the effect of surface anisotropy on the AC susceptibility and its competition with dipolar inter-particle interactions.

The paper ends with a discussion of the Vogel-Fulcher law and concluding remarks.

II. ENERGY AND EQUILIBRIUM SUSCEPTIBILITY

A. Nanoparticle assembly

We consider a monodisperse and textured assembly of \mathcal{N} ferromagnetic nanoclusters each carrying a magnetic moment $\mathbf{m}_i = m_i \mathbf{s}_i$, $i = 1, \dots, \mathcal{N}$ of magnitude m and direction \mathbf{s}_i , with $|\mathbf{s}_i| = 1$. Each magnetic moment has a uniaxial easy axis \mathbf{e} aligned along the z direction. The energy of a magnetic moment \mathbf{m}_i interacting with all the other magnetic moments within the assembly, in a magnetic field $\mathbf{H} = H\mathbf{e}_h$, reads (after multiplying by $-\beta = -1/k_B T$)

$$\mathcal{E}_i = \mathcal{E}_i^{(0)} + \mathcal{E}_i^{\text{DDI}}, \quad (1)$$

where the first contribution $\mathcal{E}_i^{(0)} = x_i \mathbf{s}_i \cdot \mathbf{e}_h + \mathcal{A}(\mathbf{s}_i)$ is the energy of the free nanocluster at site i , comprising the Zeeman energy and the anisotropy contributions from the core and surface. $\mathcal{A}(\mathbf{s}_i)$ is a function that depends on the anisotropy model and is given by

$$\mathcal{A}(\mathbf{s}_i) = \begin{cases} \sigma_i (\mathbf{s}_i \cdot \mathbf{e}_i)^2, & \text{OSP,} \\ \sigma_i \left[(\mathbf{s}_i \cdot \mathbf{e}_i)^2 - \frac{\zeta}{2} (s_{i,x}^4 + s_{i,y}^4 + s_{i,z}^4) \right], & \text{EOPS.} \end{cases} \quad (2)$$

OSP and EOSP stand respectively for One-spin problem and Effective One-spin problem which are macroscopic models used for representing the magnetic state of the nanocluster.² In the present case, we restrict ourselves to the situation where the uniaxial anisotropy axis is aligned along the z direction, *i.e.* with a common axis with the cubic anisotropy. This assumption makes the analytical calculations somewhat simpler and the physical interpretation more transparent, but it does not represent a significant discrepancy with regard to the real situation. Indeed, the uniaxial anisotropy considered in Eq. (2) is in fact an effective anisotropy that takes account of both the magneto-crystalline and shape anisotropy. In typical nanoparticle assemblies this effective anisotropy is rather strong, especially for elongated nanoparticles. As such a small tilting of the cubic anisotropy with respect to the axis of the effective uniaxial anisotropy should not change the results in a significant way. For a more general situation with an arbitrary orientation of the cubic anisotropy axes with respect to the uniaxial anisotropy axis, one can write the cubic contribution in a different reference frame (x', y', z') and then introduce in Eq. (2) a rotation matrix such that $s_{i,\alpha'} = \sum_{\beta=x,y,z} R^{\alpha\beta} s_{i,\beta}$, as was done in a different context in Ref. 24.

The second term in Eq. (1) is the dipole-dipole interaction (DDI) between nanoclusters which can be writ-

ten as $\mathcal{E}_i^{\text{DDI}} = \xi \sum_{j < i} \mathbf{s}_i \cdot \mathcal{D}_{ij} \cdot \mathbf{s}_j$, where \mathcal{D}_{ij} is the DDI tensor $\mathcal{D}_{ij} \equiv \frac{1}{r_{ij}^3} (3\mathbf{e}_{ij}\mathbf{e}_{ij} - 1)$, with $\mathbf{r}_{ij} = \mathbf{r}_i - \mathbf{r}_j$ and $\mathbf{e}_{ij} = \mathbf{r}_{ij}/r_{ij}$ is the unit vector along the i - j bond.

For convenience, we have introduced the following dimensionless parameters

$$x \equiv \frac{mH}{k_B T}, \quad \sigma \equiv \frac{K_2 V}{k_B T}, \quad \zeta \equiv \frac{K_4}{K_2}, \quad \xi \equiv \left(\frac{\mu_0}{4\pi} \right) \left(\frac{m^2/a^3}{k_B T} \right)$$

together with the DDI coefficient $\tilde{\xi} \equiv \xi \mathcal{C}^{(0,0)}$. $\mathcal{C}^{(0,0)} = -4\pi (D_z - \frac{1}{3})$ and D_z is the demagnetizing factor along the z axis. K_2, K_4 are the constants of the uniaxial and cubic anisotropy, respectively. a is the “super-lattice” parameter or the inter-particle distance in the assembly whose particles are supposed to occupy a simple cubic (SC) lattice. Yet, we stress that a generalization to other super-lattices (FCC, BCC, ...) is rather straightforward. One should simply re-evaluate the lattice sums $\mathcal{C}^{(0,0)}$ for the given super-lattice. Similarly, one could easily mimic a disordered spatial arrangement by an evaluation of $\mathcal{C}^{(0,0)}$ in the case of a randomly depleted lattice. However, for the sake of clarity and to keep our discussion simple we will consider the SC case in the rest of this paper.

The (dimensionless) DDI field Ξ_i acting on the magnetic moment \mathbf{m}_i reads

$$\Xi_i = \xi \sum_j \mathcal{D}_{ij} \cdot \mathbf{s}_j. \quad (3)$$

Later we make use of the spin average $\langle \Xi_{i,\parallel}^2 \rangle_0$, where $\Xi_{i,\parallel} = \Xi_i \cdot \mathbf{e}_i$ is the longitudinal component of Ξ_i , which is defined by

$$\langle \Xi_{i,\parallel}^2 \rangle_0 \equiv \frac{1}{4\pi} \int \left(\prod_j d\mathbf{s}_j \right) \Xi_{i,\parallel}^2 e^{\sum_j \mathcal{E}_j^{(0)}}. \quad (4)$$

The average $\langle \rangle_0$ is defined with respect to the Gibbs probability distribution containing only the energy contributions pertaining to a free cluster. Finally, the spin average of the transverse component of Ξ_i can be obtained from the identity $\langle \Xi_{i,\perp}^2 \rangle_0 = \langle \Xi_i^2 \rangle_0 - \langle \Xi_{i,\parallel}^2 \rangle_0$.

B. Statement of the problem

In the present work we shall be concerned with the study of the combined effects of surface anisotropy and dipolar interactions on the dynamic susceptibility of an assembly of monodisperse nanoclusters with oriented uniaxial anisotropy. The cubic anisotropy which stems from spin non-collinearities on the cluster’s surface is assumed to have its axes parallel to the crystal axes. We then derive analytical formulas in several cases of low field ($x \ll 1$), high-energy barrier ($\sigma \gg 1$), small surface anisotropy ($|\zeta| < 1$) and weak DDI ($\xi \ll 1$). In particular, for the calculation of the spin averages (4) and

kindred ones we will drop all terms of orders higher than 2. For this reason, it turns out that the calculation of such averages can be done with good approximation with only the uniaxial anisotropy contribution in the Gibbs probability distribution.² The final results are expressed in the end in terms of the following well known averages (obtained in the absence of a magnetic field) $\langle s_i^\alpha \rangle_0 = 0$, and

$$\langle s_j^\alpha s_k^\beta \rangle_0 = \left[\frac{1}{3}(1 - S_{j2})\delta^{\alpha\beta} + S_{j2}e_j^\alpha e_j^\beta \right] \delta_{jk} \quad (5)$$

with^{15,25}

$$S_{il}(\sigma_i) \simeq \begin{cases} \frac{(l-1)!!}{(2l+1)!!} \left(\frac{\sigma_i}{2}\right)^{l/2} + \dots, & \sigma_i \ll 1, \\ 1 - \frac{l(l+1)}{4\sigma_i} + \dots, & \sigma_i \gg 1. \end{cases} \quad (6)$$

C. Equilibrium susceptibility

For a weakly interacting assembly of nanoclusters described with the help of the EOSP model, the equilibrium susceptibility reads (to first order in ξ)

$$\chi^{\text{eq}}(x, \sigma, \zeta, \tilde{\xi}) \simeq \chi_{\text{free}}^{\text{eq}} + \tilde{\xi} \chi_{\text{int}}^{\text{eq}} \quad (7)$$

where $\chi_{\text{free}}^{\text{eq}}$ is the equilibrium (linear) susceptibility of the non-interacting assembly in the limit of high anisotropy energy barrier^{2,25}

$$\chi_{\text{free}}^{\text{eq}}(x, \sigma, \zeta) = 2\chi_0^\perp \sigma \left[\chi_{\text{free}}^{(1)} + 3\chi_{\text{free}}^{(3)} x^2 \right], \quad (8)$$

$$\begin{aligned} \chi_{\text{free}}^{(1)} &= \left(1 - \frac{1}{\sigma}\right) + \frac{\zeta}{\sigma} \left(-1 + \frac{2}{\sigma}\right), \\ \chi_{\text{free}}^{(3)} &= \frac{1}{3} \left[\left(-1 + \frac{2}{\sigma}\right) + \frac{\zeta}{\sigma} \left(2 - \frac{5}{\sigma}\right) \right]. \end{aligned}$$

Here χ_0^\perp is the transverse equilibrium susceptibility per spin at zero temperature in the absence of a bias field

$$\chi_0^\perp \equiv \left(\frac{\mu_0 m^2}{2K_2 V} \right).$$

This can be obtained from Eq. (3.86) of Ref. 26 upon setting the field to zero.

The contribution of DDI to the equilibrium susceptibility is given by²

$$\chi_{\text{int}}^{\text{eq}}(x, \sigma, \zeta) = 2\chi_0^\perp \sigma \left[\chi_{\text{int}}^{(1)} + 3\chi_{\text{int}}^{(3)} x^2 \right], \quad (9)$$

$$\begin{aligned} \chi_{\text{int}}^{(1)} &= 1 - \frac{2}{\sigma} - 2 \left(1 - \frac{3}{\sigma}\right) \frac{\zeta}{\sigma}, \\ \chi_{\text{int}}^{(3)} &= -\frac{4}{3} \left[\left(1 - \frac{3}{\sigma}\right) - \frac{3\zeta}{\sigma} \right]. \end{aligned}$$

In the sequel, all susceptibilities will be measured in units of χ_0^\perp .

III. AC SUSCEPTIBILITY

The dynamic response of the EOSP assembly can be studied with the help of the AC susceptibility. For an arbitrary angle ψ between the (common) easy axis and the field direction, the effective susceptibility may be written as $\chi = \chi_{\parallel} \cos^2 \psi + \chi_{\perp} \sin^2 \psi$.

Shliomis and Stepanov²⁷ proposed a simple Debye form for $\chi(\omega)$ which can be generalized to describe the effect of a longitudinal bias field by writing

$$\chi = \frac{\chi_{\parallel}(T, H)}{1 + i\omega\tau_{\parallel}} \cos^2 \psi + \frac{\chi_{\perp}(T, H)}{1 + i\omega\tau_{\perp}} \sin^2 \psi, \quad (10)$$

where τ_{\parallel} and τ_{\perp} are appropriate longitudinal (inter-well) and transverse (intra-well) relaxation times; $\chi_{\parallel}(T, H)$ and $\chi_{\perp}(T, H)$ are respectively the longitudinal and transverse components of the equilibrium susceptibility.

For an assembly with oriented anisotropy in a longitudinal field ($\psi = 0$), we may assume that the transverse response is instantaneous, *i.e.* $\tau_{\perp} = 0$. In this case the AC susceptibility is given by Eq. (10) or using $\tau_{\parallel} = \Gamma^{-1}$ and $\chi_{\parallel} = \chi^{\text{eq}}$ defined in Eq. (7),

$$\chi(x, \sigma, \zeta, \tilde{\xi}, \eta) = \frac{\chi^{\text{eq}}}{1 + i\omega\Gamma^{-1}}. \quad (11)$$

Next, we introduce the reduced frequency

$$\eta(x, \sigma, \zeta, \tilde{\xi}, \lambda) \equiv \omega\tau_{\parallel} = (\omega\tau_D)(\tau_D\Gamma)^{-1}, \quad (12)$$

with λ being the damping parameter. $\Gamma(x, \sigma, \zeta, \tilde{\xi}, \lambda)$ is the relaxation rate of an EOSP nanocluster weakly interacting within the assembly; $\tau_D = (\lambda\gamma_{\text{gyr}} H_K)^{-1}$ is the free diffusion time, $H_K = 2K_2 V/M$ the (uniaxial) anisotropy field, and $\gamma_{\text{gyr}} \simeq 1.76 \times 10^{11} \text{ (T.s)}^{-1}$ the gyromagnetic ratio. For example, for cobalt particles the anisotropy field is $H_K \sim 0.3 \text{ T}$, and for $\lambda = 0.1 - 10$, $\tau_D \sim 2 \times 10^{-10} - 2 \times 10^{-12} \text{ s}$.

At this point, the only missing ingredient to evaluate the susceptibility in Eq. (11) is the relaxation rate. Therefore, the next Section is devoted to the calculation of the relaxation rate $\Gamma(x, \sigma, \zeta, \tilde{\xi}, \lambda)$.

A. Relaxation rate

Here we derive an expression for the relaxation rate of a weakly interacting EOSP nanocluster.

In Ref. 11 Jönsson and Garcia-Palacios derived the following approximate expression for Γ

$$\Gamma \simeq \Gamma_0 \left[1 + \frac{1}{2} \langle \Xi_{\parallel}^2 \rangle_0 + \frac{1}{4} F(\alpha) \langle \Xi_{\perp}^2 \rangle_0 \right]. \quad (13)$$

This takes account of the various approximations stated earlier inasmuch as the general spin averages $\langle \dots \rangle$

are replaced by their analogs $\langle \dots \rangle_0$ defined in Eq. (4). Γ_0 is the relaxation rate in the absence of DDI. The function $F(\alpha)$ is given by²⁸

$$F(\alpha) = 1 + 2(2\alpha^2 e)^{1/(2\alpha^2)} \gamma\left(1 + \frac{1}{2\alpha^2}, \frac{1}{2\alpha^2}\right), \quad (14)$$

with $\gamma(a, z) = \int_0^z dt t^{a-1} e^{-t}$ the incomplete gamma function, and where $\alpha = \lambda\sqrt{\sigma}$. In Ref. 11 the free-particle relaxation rate Γ_0 was given in the absence of the applied magnetic field, *i.e.* $\tau_D \Gamma_0 = \frac{2}{\sqrt{\pi}} \sigma^{1/2} e^{-\sigma}$. A more general expression for the free-particle relaxation rate in a longitudinal magnetic field is the Néel-Brown formula²⁹

$$\tau_D \Gamma_{\text{NB}} = \frac{\sigma^{1/2} (1 - h^2)}{\sqrt{\pi}} \times \left[(1 + h) e^{-\sigma(1+h)^2} + (1 - h) e^{-\sigma(1-h)^2} \right], \quad (15)$$

with $h \equiv x/2\sigma$. Setting $h = 0$ recovers the previous expression.

The relaxation rate (15) has to be generalized for the present purposes in order to take into account surface anisotropy, in addition to the magnetic field as well as the core anisotropy.

For intermediate-to-high damping Langer's approach allows us to compute the relaxation rate Γ of a system with many degrees of freedom related with its transition from a metastable state through a saddle point³⁰⁻³⁵

$$\Gamma = \frac{|\kappa|}{2\pi} \frac{\tilde{Z}_s}{Z_m}, \quad (16)$$

where Z_m and \tilde{Z}_s are respectively the partition functions in the vicinity of the energy metastable minimum and the saddle point. The two partition functions are computed using a quadratic expansion of the energy at the corresponding stationary states. The attempt frequency κ is computed upon linearizing the dynamical equation around the saddle point, diagonalizing the resulting matrix and selecting its negative eigenvalue.^{30,31}

The dynamics of a single magnetic moment is governed by the (damped) Landau-Lifshitz equation and Langer's (or Néel-Brown) expression renders the relaxation rate for its escape from the minimum $(\theta^{(m)}, \varphi^{(m)})$ through the saddle point $(\theta^{(s)}, \varphi^{(s)})$, in the limit of intermediate-to-high damping. Owing to the approximations adopted in this work, especially the smallness of the surface anisotropy with respect to the uniaxial anisotropy ($|\zeta| < 1$), the energy potential of the non-interacting cluster presents two global minima that are mainly defined by the uniaxial anisotropy, as is shown in Fig. 1 (in zero field), while the surface anisotropy induces saddle points at the equator. In the present case, changing the sign of ζ does not affect the loci of the minima but those of the saddle points are rotated by $\pi/4$ around the z axis. The overall shape of the energy landscape remains, though,

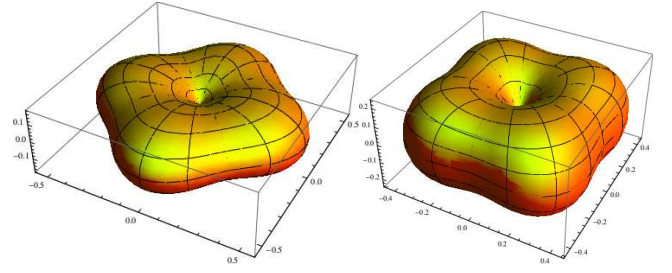


Figure 1: Energy landscape at zero field in the limit of a large uniaxial anisotropy, for $\zeta > 0$ (left), and $\zeta < 0$ (right).

quite similar. The global minima are $\theta^{(m)} = 0, \pi$ with uniaxial symmetry around the z axis. Then, we have

$$Z_m \simeq \frac{2\pi}{2\sigma(1 - \zeta - h)} e^{\mathcal{E}_m^{(0)}}, \quad (17)$$

where $\mathcal{E}_m^{(0)} = 2\sigma \times \frac{1}{4} (2 - \zeta - 4h)$ is the energy at the metastable minimum $\theta^{(m)} = \pi$.

There are four equivalent escape routes (saddle points) related to each other by a rotational symmetry with respect to the azimuthal angle φ and their loci depend on the sign of ζ . Indeed, for $\zeta > 0$ we have $\varphi^{(s)} = \frac{\pi}{4}, \frac{3\pi}{4}, \frac{5\pi}{4}, \frac{7\pi}{4}$ and

$$\cos \theta^{(s)} = \sqrt{\frac{2 + \zeta}{3\zeta}} \sin\left(\frac{\phi}{3}\right) - \sqrt{\frac{2 + \zeta}{9\zeta}} \cos\left(\frac{\phi}{3}\right) \quad (18)$$

with $\cos \phi = \frac{9h\zeta^{1/2}}{(2 + \zeta)^{3/2}}$.

For $\zeta < 0$ the saddle points are given by $\varphi^{(s)} = 0, \frac{\pi}{2}, \pi, \frac{3\pi}{2}$ and

$$\cos \theta^{(s)} = \left[\frac{h}{4\zeta} + \sqrt{\Delta} \right]^{1/3} + \left[\frac{h}{4\zeta} - \sqrt{\Delta} \right]^{1/3} \quad (19)$$

with $\Delta = \left(\frac{h}{4\zeta} \right)^2 - \left(\frac{1 + \zeta}{6\zeta} \right)^3$.

For a small magnetic field h , the azimuthal angle at the saddle point remains close to the equator while an expansion of Eq. (18) yields $\theta^{(s)} \simeq \frac{\pi}{2} + \frac{2h}{2 + \zeta}$. It is worth mentioning that the symmetry breaking of the continuous rotation around φ , induced by the introduction of a cubic anisotropy, appears as soon as ζ assumes a finite value. However, for very small values of ζ the energy surface around the saddle points remains flat rendering the quadratic expansion of the energy at the saddle point questionable [see Fig. 2 below]. As a consequence Langer's approach does not apply in such situations, as was emphasized earlier.^{36,37}

Next, expanding the energy at the saddle points for $\zeta > 0$ and $\zeta < 0$ (with not too small $|\zeta|$) we obtain the following generic expression for the relaxation rate (upon mul-

tipling by the symmetry factor 4) $\Gamma_0 = \Gamma_{(\pi,0) \rightarrow (\theta^{(s)}, \varphi^{(s)})}$

$$\tau_D \Gamma_0 = 4 \times \frac{|\kappa|}{2\pi} \sin \theta^{(s)} \frac{2\sigma(1 - \zeta - h)}{\sqrt{|\mu_1^{(s)} \mu_2^{(s)}|}} e^{\Delta \mathcal{E}^{(0)}}. \quad (20)$$

The attempt frequency κ , as a function of the damping parameter λ , is given by the general expression

$$\kappa = \frac{\lambda}{2} \times \left[\frac{(\mu_2^{(s)} + \mu_1^{(s)})}{\sqrt{(\mu_2^{(s)} + \mu_1^{(s)})^2 - 4(1 + \frac{1}{\lambda^2}) \mu_1^{(s)} \mu_2^{(s)}}} \right] \quad (21)$$

where $\mu_i^{(s)}, i = 1, 2$ are the eigenvalues of the energy quadratic form near the saddle point, with respect to the variables θ, φ , respectively. These, together with the energy at the saddle point, are given by

$$\mathcal{E}_s^{(0)} = 2\sigma \left[h \cos \theta^{(s)} + \frac{1}{2} \cos^2 \theta^{(s)} - \frac{\zeta}{8} (\sin^4 \theta^{(s)} + 2 \cos^4 \theta^{(s)}) \right]$$

$$\mu_1^{(s)} = 2\sigma \times \frac{-1}{4} \left[4h \cos \theta^{(s)} + (4 - \zeta) \cos 2\theta^{(s)} - 3\zeta \cos 4\theta^{(s)} \right]$$

$$\mu_2^{(s)} = 2\sigma \left[-\zeta \sin^4 \theta^{(s)} \right].$$

for $\zeta > 0$.

As the energy landscape remains globally the same by changing $\zeta \rightarrow -\zeta$, only the energy at the saddle points and the eigenvalues change, yet the overall form of the relaxation rate is still given by Eqs. (20) and (21) with the following substitutions

$$\mathcal{E}_s^{(0)} = 2\sigma \left[h \cos \theta^{(s)} + \frac{1}{2} \cos^2 \theta^{(s)} - \frac{\zeta}{4} (\cos^4 \theta^{(s)} + \sin^4 \theta^{(s)}) \right],$$

$$\mu_1^{(s)} = 2\sigma \left[-h \cos \theta^{(s)} - \cos(2\theta^{(s)}) + \zeta \cos(4\theta^{(s)}) \right],$$

$$\mu_2^{(s)} = 2\sigma \left[\zeta \sin^4 \theta^{(s)} \right].$$

for $\zeta < 0$.

Finally, the energy barrier $\Delta \mathcal{E}^{(0)}$ in Eq. (20) is defined as $\Delta \mathcal{E}^{(0)} = \mathcal{E}_s^{(0)} - \mathcal{E}_m^{(0)}$.

In the limit of zero field ($h = 0$) and for $\zeta > 0$, for instance, $\mu_1^{(s)}/2\sigma \rightarrow (\zeta + 2)/2$, $\mu_2^{(s)}/2\sigma \rightarrow \zeta$, $\mathcal{E}_0^{(s)}/2\sigma \rightarrow -\zeta/8$ so that the relaxation rate in (20) reduces to the result obtained in Ref. 37, normalized with respect to the Néel's free-diffusion relaxation time¹⁷ $\tau_N = \frac{m}{2\alpha\gamma k_B T} = \sigma\tau_D$.

Two remarks are in order:

- There are two limits to the range of ζ (> 0). First, ζ must not exceed some value that marks the limit of validity of the EOSP model. From numerical calculations,^{4,6} this has been evaluated to ~ 0.25 for an SC lattice and ~ 0.35 for an FCC lattice. The second limit stems from the fact that the analytical expressions obtained above for Γ within Langer's approach cannot be continued to $\zeta = 0$

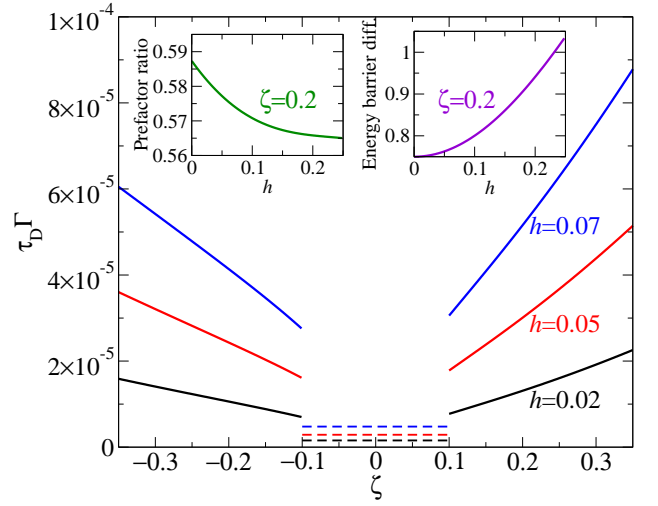


Figure 2: Relaxation rate as a function of the (negative and positive) parameter ζ , for three values of the (reduced) applied field h : Full lines correspond to the relaxation rate defined in Eq. (22), while the dashed lines are plots of the ζ -independent Néel-Brown relaxation rate (15) for different values of the magnetic field. Insets: Ratio of the two prefactors $\Gamma_p^+(h, \sigma, \zeta, \lambda)/\Gamma_p^-(h, \sigma, \zeta, \lambda)$, as defined in Eq. (22), and energy barrier difference against h , for $\sigma = 15$ and $\zeta = 0.2$.

because the saddle points created by the cubic contribution to the anisotropy disappear at the uniaxial anisotropy limit. The lower limit on ζ can be obtained by setting to zero the first derivative of Γ with respect to ζ and numerically solving the ensuing equation. Doing so, we find that for $\sigma = 15 \dots 25$, for instance, ζ_{crit} is of the order of 0.1.

- Because of the non-axial symmetry (owing to the presence of surface cubic anisotropy) considered here, the relaxation rate depends in a non trivial way on the damping parameter. Consequently, the longitudinal response (in-phase and out-of-phase) are damping-dependent.

In Fig. 2 we plot the relaxation rate for both $\zeta > 0$ and $\zeta < 0$ as a function of ζ and different values of the applied field h , for $\sigma = 15$. In this case, as mentioned above, the relaxation rate computed within our approach is only valid for $0.1 < |\zeta| < 1$. For smaller values of $|\zeta|$ Langer's approach is no longer valid and the relaxation rate is given by the Néel-Brown formula (15) which does not depend on ζ . This is shown by the dashed lines in Fig. 2. As it can be expected, the relaxation rate that includes the cubic anisotropy is larger than the Néel-Brown relaxation rate since the creation of saddle points increases the probability of escaping from the metastable state.

Next, if we write the relaxation rates given by Eq. (20) in the form

$$\Gamma_0(h, \sigma, \zeta, \lambda) = \Gamma_p^\epsilon(h, \sigma, \zeta, \lambda) e^{\Delta \mathcal{E}_\epsilon^{(0)}(\zeta)} \quad (22)$$

with $\epsilon = +$ for $\zeta > 0$ and $\epsilon = -$ for $\zeta < 0$ we can study

the behavior of the ratio of the prefactors and the difference of the energy barriers as the field is varied. The corresponding plots are given in the inset in Fig. 2. We see that the ratio of the prefactors is a decreasing function of h while the difference of the energy barriers is an increasing function thereof. This implies that there is a competition between the prefactor-dominated dynamics and the relaxation through the energy-barrier crossing, or in other words, between the dynamics dominated respectively by the fluctuations of the transverse and the longitudinal components of the magnetic moment.

Caution is necessary when trying to compare the expression of the relaxation rate $\Gamma_0(h, \sigma, \zeta, \lambda)$ derived here in the presence of both surface effects ($\zeta \neq 0$) and DDI ($\xi \neq 0$) with the relaxation rate obtained, in the absence of the cubic anisotropy, by other authors.^{11,38} Indeed, in the presence of an arbitrary magnetic field, one cannot simply set $\zeta = 0$ in our expressions because these have been derived using Langer's approach that relies on the validity of the quadratic expansion of the energy at the minima and saddle points; a validity that breaks down for rather small (but non vanishing) values of ζ . From a mathematical point of view, setting ζ to zero in Eqs. (18, 19), for example, leads to a singularity.

Now, for the assembly we use the spin averages $\langle \Xi_{i,\parallel}^2 \rangle_0$ and $\langle \Xi_{i,\perp}^2 \rangle_0$ obtained in Ref. 11 for a monodisperse assembly on a SC lattice and in the absence of an external magnetic field

$$\begin{aligned} \langle \Xi_{i,\parallel}^2 \rangle_0 &= \frac{\xi^2}{3} [(1 - S_2) \mathcal{R} + 3S_2 \mathcal{T}], \\ \langle \Xi_{i,\perp}^2 \rangle_0 &= \frac{\xi^2}{3} [(2 + S_2) \mathcal{R} - 3S_2 \mathcal{T}], \end{aligned} \quad (23)$$

where S_2 is defined in Eq. (6). \mathcal{R} and \mathcal{T} are lattice sums given by $\mathcal{R} = 2 \sum_{j \neq i} r_{ij}^{-6}$, $\mathcal{T} = \sum_{j \neq i} (\mathbf{e} \cdot \mathcal{D}_{ij} \mathbf{e})^2$. For a simple cubic lattice we have, in the thermodynamic limit, $\mathcal{R} \simeq 16.8$, $\mathcal{T} \simeq 13.4$.

Therefore, using Eqs. (14), (20), and (23) in Eq. (13) we obtain the relaxation rate for an assembly of interacting clusters within the EOSP approach

$$\Gamma(h, \sigma, \zeta, \lambda, \xi) \simeq \Gamma_0(h, \sigma, \zeta, \lambda) \left[1 + \frac{\xi^2}{6} \mathcal{S}(\lambda) \right]. \quad (24)$$

where $\mathcal{S}(\lambda)$ is defined by

$$\mathcal{S}(\lambda) = (1 + F(\lambda)) \mathcal{R} + (3\mathcal{T} - \mathcal{R}) \left(1 - \frac{F(\lambda)}{2} \right) S_2. \quad (25)$$

Alternatively, using $\eta_0 = \omega \Gamma_0^{-1}$, we can also rewrite Eq. (12) as

$$\eta(h, \sigma, \zeta, \xi, \lambda) = \eta_0(h, \sigma, \zeta, \lambda) \left[1 + \frac{\xi^2}{6} \mathcal{S}(\lambda) \right]. \quad (26)$$

B. AC susceptibility

We rewrite the AC susceptibility (11) separating its real and imaginary parts $\chi(h, \sigma, \zeta, \xi, \eta) = \chi' - i\chi''$ with

$$\chi' = \chi^{\text{eq}} \frac{1}{1 + \eta^2}, \quad \chi'' = \chi^{\text{eq}} \frac{\eta}{1 + \eta^2}. \quad (27)$$

Now, we substitute for χ^{eq} and η their respective expressions (7) and (26), taking account of DDI and surface anisotropy contributions given above. We obtain

$$\begin{aligned} \chi' &\simeq \chi'_{\text{free}} + \frac{\xi}{1 + \eta_0^2} \left[\Lambda^{(1)} + \xi \frac{\eta_0^2}{1 + \eta_0^2} \Lambda^{(2)} \right], \\ \chi'' &= \chi''_{\text{free}} + \frac{\xi \eta_0}{1 + \eta_0^2} \left[\Lambda^{(1)} + \xi \frac{1 - \eta_0^2}{1 + \eta_0^2} \Lambda^{(2)} \right], \end{aligned}$$

where we have defined the in-phase and out-of-phase susceptibilities in the absence of DDI

$$\chi'_{\text{free}}(h, \sigma, \zeta, \lambda) \equiv \frac{\chi_{\text{free}}^{\text{eq}}}{1 + \eta_0^2}, \quad \chi''_{\text{free}}(h, \sigma, \zeta, \lambda) \equiv \frac{\eta_0 \chi_{\text{free}}^{\text{eq}}}{1 + \eta_0^2}$$

together with the 1st- and 2nd-order DDI contributions

$$\Lambda^{(1)} \equiv \chi_{\text{int}}^{\text{eq}} \mathcal{C}^{(0,0)},$$

$$\Lambda^{(2)} \equiv \frac{\chi_{\text{free}}^{\text{eq}}}{3} \mathcal{S}(\lambda).$$

$\chi_{\text{free}}^{\text{eq}}$ and $\chi_{\text{int}}^{\text{eq}}$ are given by Eqs. (8, 9) and $\eta_0 = \omega \Gamma_0^{-1}$ by Eq. (20).

IV. RESULTS

A. Noninteracting assembly of OSP nanomagnets

Using our formalism we first reproduce the well known results for the in-phase and out-of-phase susceptibilities for an assembly of noninteracting nanomagnets with uniaxial anisotropy, in zero DC field.^{17,26} In Fig. 3 we plot the in-phase (left) and out-of-phase (right) susceptibilities as functions of $1/\sigma \propto T$ for zero field ($x = 0$) and different frequencies. On the left we have also included the equilibrium susceptibility $\chi_{\text{free}}^{\text{eq}}$ ($\zeta = 0$), represented by the solid line.

The appearance in χ' and χ'' of a maximum at some particular temperature T_{max} and the displacement of the latter to the right (higher temperatures) upon increasing the measuring frequency is already well understood and explained in details, *e.g.* in Ref. 17. In particular, the maximum of χ' is formed as a result of the competition between the blocking effect (namely the decrease of the relaxation rate) and the increase of χ^{eq} as the temperature decreases. At low temperature, the relaxation time is longer than the measuring time $t_m = 2\pi/\omega$ and

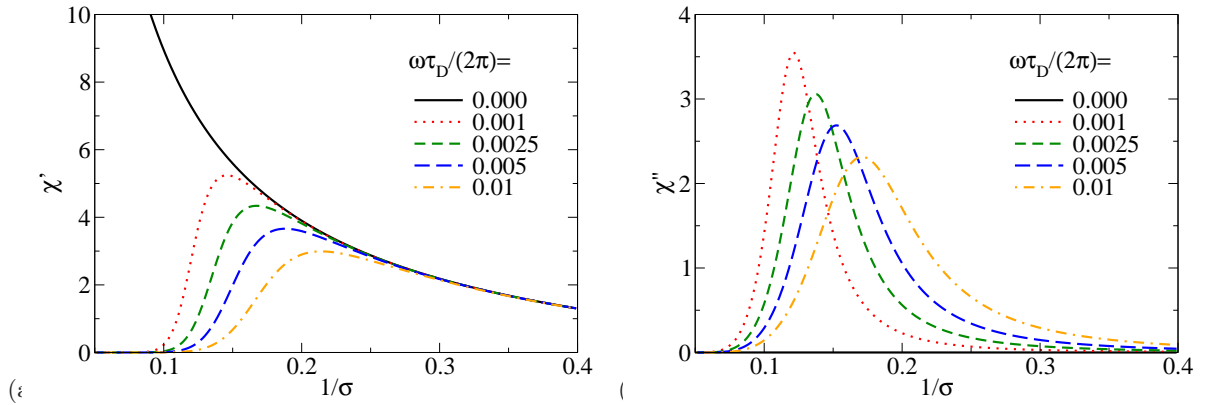


Figure 3: (a) χ' (left) and (b) χ'' for a free assembly ($\xi = 0$) within the OSP model, *i.e.* without surface anisotropy ($\zeta = 0$), for different frequencies $\tilde{f} \equiv \omega\tau_D/(2\pi)$.

thereby over a large number of cycles of the AC field, the over-barrier switching probability is nearly zero and the response consists mainly of intra-well rotations. As T increases the clusters magnetic moments start to depart from their respective energy minima due to thermal fluctuations. Then, over the same number of cycles of the AC field the switching probability acquires a non negligible value. The response starts to increase with increasing temperature within a range where the thermally-activated mechanism of over-barrier crossing is not yet efficient enough, leading to a considerable delay of the response with respect to the excitation. This leads to a considerable out-of-phase response χ'' as witnessed by the increase of the latter, see Fig. 3 (right). At higher temperatures, the over-barrier crossing mechanism becomes so efficient that the magnetic moments instantaneously distribute themselves among the various energy minima, in phase with the probing field. At much higher temperatures, the distribution of the magnetic moments reaches its equilibrium state and the χ' curves become independent of the measuring frequency and superimpose on the equilibrium linear susceptibility χ^{eq} , and correspondingly χ'' tends to zero.

The displacement of T_{max} is easily understood from the expression of the latter as a function of the measuring frequency ν_m . Indeed, this temperature is related with the over-barrier rotation process whose relaxation time is approximately given by the simple Arrhenius law $\tau_{\parallel} = \tau_0 \exp(\Delta E/k_B T)$, where ΔE is the effective energy barrier and $\tau_0 \sim 10^{-12} - 10^{-9}$ s the characteristic time of the intra-well dynamics. At $T = T_{\text{max}}$ we can write $\tau_{\parallel} \simeq t_m$, *i.e.* the measuring time (~ 100 s for a commercial SQUID), and this then leads to

$$T_{\text{max}} = \frac{\Delta E}{k_B} \times \ln^{-1} \left(\frac{\tau_m}{\tau_0} \right). \quad (28)$$

From this relation, one can easily infer the increase of T_{max} as the measuring frequency $\nu_m = \tau_m^{-1}$ increases. From the physical viewpoint, with higher ν_m one probes on average more probable (with higher relaxation rate)

switching processes and this is in effect induced by an increase in temperature.

B. Noninteracting assembly: effects of surface anisotropy

Now, to investigate the effect of surface anisotropy on the AC susceptibility we can compute the real and imaginary components of the latter as functions of temperature, for different values of the parameter $\zeta > 0$.

We have observed that the maxima of both χ' and χ'' shifts toward higher temperatures as ζ increases. Indeed, setting to zero the first derivative of χ' with respect to temperature and setting $T = T_{\text{max}}$ in the ensuing equation, we can solve the latter for T_{max} as a function of the other parameters, especially ζ . We indeed find a monotonously increasing function of ζ . Intuitively this result appears to be at variance with the fact that since the cubic (surface) anisotropy creates saddle points it leads to an increase of the relaxation rate and thereby to a decrease of T_{max} . However, as mentioned earlier the location of the maximum of the dynamic response, while it does depend on the energy barriers, it is strongly dependent on the equilibrium response (*i.e.* χ^{eq}) which is rather different for the pure uniaxial case ($\zeta = 0$). More precisely, χ^{eq} is a decreasing function of ζ and thereby when ζ increases the dynamic response requires higher temperatures to reach its maximum, thus leading to an increasing T_{max} for increasing ζ .

C. Effects of inter-particle interactions in the absence of surface anisotropy

The effect of DDI on the AC susceptibility has been widely investigated by many groups.^{11,12,16,18,39-47} In Ref. 47 the authors provide a short review of the situation regarding the effect of DDI on the maximum of χ' and χ'' and their shift in temperature as the DDI inten-

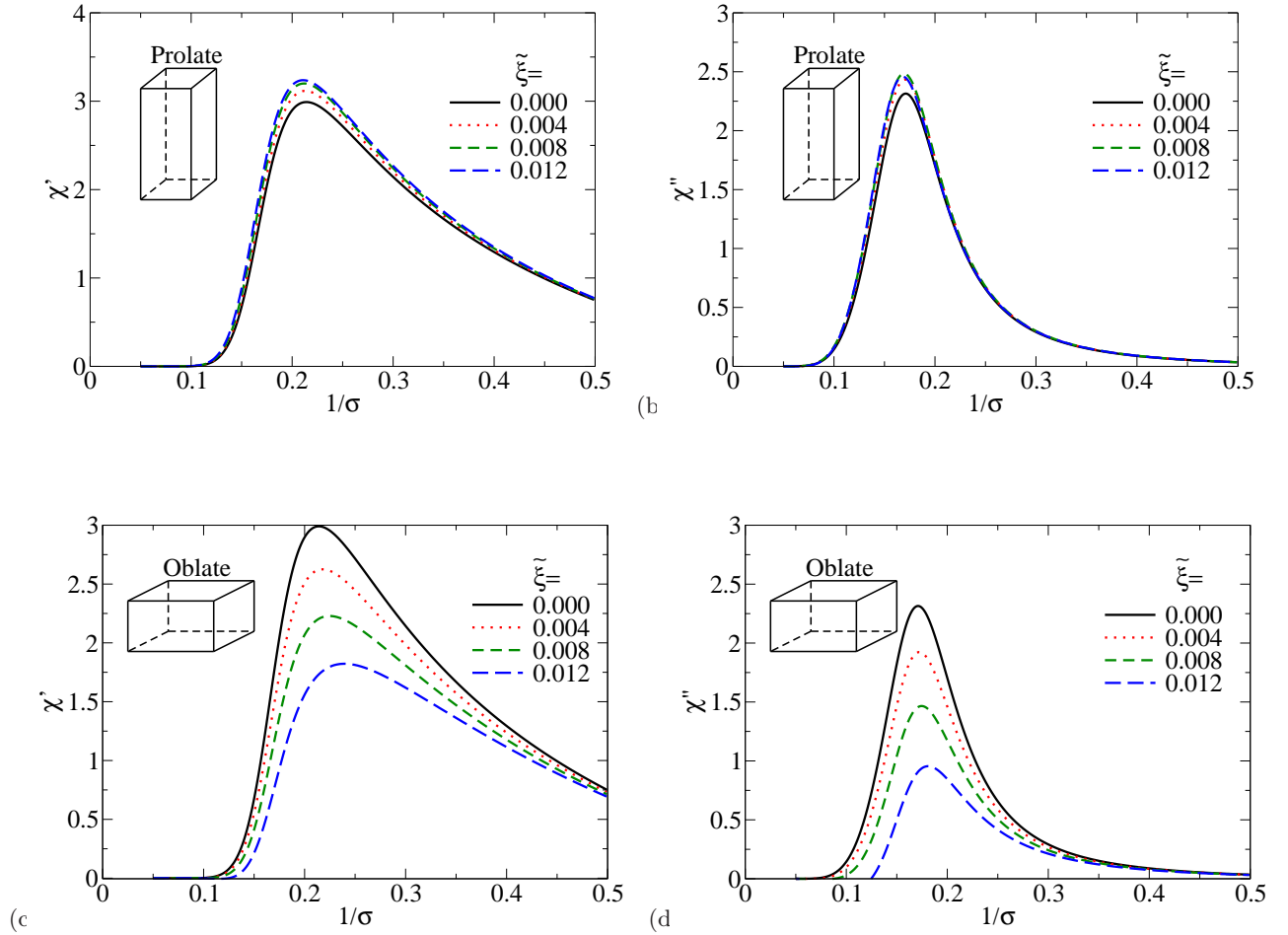


Figure 4: (a) χ' and (b) χ'' for an interacting prolate ($10 \times 10 \times 20$) assembly with varying DDI strength $\tilde{\xi}$, for the frequency $\tilde{f} \equiv \omega\tau_D/(2\pi) = 0.01$ in the absence of an external field $h = 0$, in the high damping regime $\lambda = 10$. Same plots in (c) and (d) for an oblate ($20 \times 20 \times 5$) assembly.

sity is varied and the assembly shape changed from oblate to prolate. It was argued that the discrepancy of conclusions found in the literature as to whether the DDI shift the maximum of χ' and χ'' towards higher or lower temperatures resides in many reasons, mostly related with the effects of damping, the shape of the (assembly) sample, and anisotropy. Here we use the same formalism and approximations and obviously confirm the same results. Therefore, we shall not repeat the conclusions of the previous work.

Nevertheless, Fig. 4 shows that as the shape of the assembly changes from prolate to oblate, we obtain an opposite shift in temperature in both the maximum of χ' and χ'' and also in the corresponding T_{\max} . In the case of isotropic samples, such as cubes, the lattice sum $\mathcal{C}^{(0,0)}$ vanishes leading to a DDI coefficient $\tilde{\xi} = 0$. Therefore, no shift is observed and the DDI do not contribute, within the present approach. For prolate and oblate samples, both shifts are explained by the fact that the equilibrium susceptibility increases with DDI in a prolate sample whereas it decreases in an oblate sample. More importantly, it is seen that the effect of DDI is

more pronounced in the oblate case because there the DDI are in competition with the uniaxial anisotropy and thus strongly contribute to suppress the equilibrium susceptibility. The effect of damping, while remaining secondary as compared to that of the assembly shape, seems to be somewhat more pronounced in the case of prolate samples. This may be due again to the fact that in the prolate case the increase of χ^{eq} with DDI is slower than its decrease for the oblate shape. As such, χ' and χ'' , and more so for χ' , are more sensitive to the change of the relaxation rate which then starts to prevail, and which does depend on damping.

D. DDI versus surface effects

Now we are ready to investigate the interplay between inter-particle DDI and intrinsic surface anisotropy. We only present the case of $\zeta > 0$ in which surface (cubic) anisotropy favors the magnetic alignment along the cube diagonals. In order to deal with the case $\zeta < 0$ one has

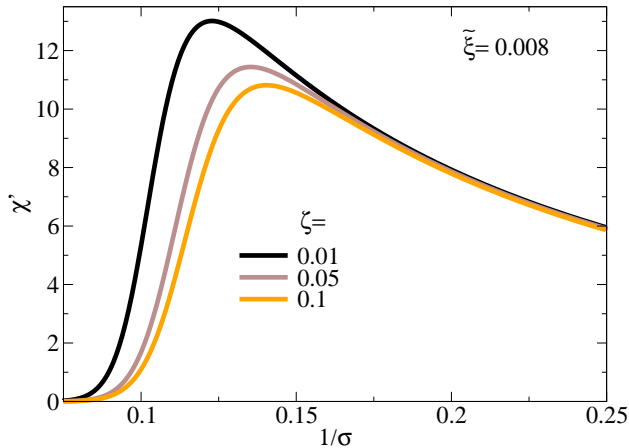


Figure 5: χ'' for an interacting prolate ($10 \times 10 \times 20$) assembly with a fixed DDI strength $\tilde{\xi} = 0.008$ and varying surface anisotropy coefficient ζ , for the frequency $\tilde{f} \equiv \omega\tau_D/(2\pi) = 0.01$. $h = 0$.

to use the corresponding relaxation rate, as discussed in Section III A. Yet, as shown in Fig. 2 the behavior of the relaxation rate for $\zeta < 0$ is qualitatively the same as that for $\zeta > 0$ and that even quantitatively the difference is not really significant. Therefore, in the remaining part of the paper we will focus our discussion on $\zeta > 0$.

We have systematically analyzed χ' and χ'' for various values of the surface anisotropy coefficient ζ , for both prolate and oblate assemblies. We have observed the upward shift of T_{\max} as ζ increases and the downward shift of the maximum of χ' and χ'' , as already discussed earlier. However, owing to the fact that the effect of increasing ζ is to draw the particle's magnetic moment towards the cube diagonals, it basically plays the same role in a prolate sample where the magnetization is enhanced along the z axis, or in an oblate sample where the magnetization is enhanced in the xy plane.

The effect of increasing the strength of DDI alone is shown in Fig. 4. In the case of a prolate sample, we have observed a shift of the maximum toward lower temperatures, in the absence of surface anisotropy. Note again that this is not the $\zeta = 0$ limit of the expressions of Section III A. It is simply the OSP model with the relaxation rate (15). The effect of frequency observed by Lee *et al.*⁴⁸ is similar to the behavior that we observe here: T_{\max} increases and χ' decreases. Furthermore, the fact that T_{\max} increases as the concentration increases is in line with what we observe for oblate samples and corresponds to the type of samples investigated by Lee *et al.* Despite the relative success of our model in interpreting the experimental data, one has to be careful as not to push the comparison too far because our approach has been derived for textured monodisperse assemblies and, more importantly, is perturbative and thus inherently restricted to weak DDI. This is in general not the case in experiments where the assemblies are often random and rather dense. In such cases (especially high

densities), a more quantitative comparison with experiments can only be accessible with the help of numerical investigations^{23,49}.

In Fig. 5 we present a specific case in order to highlight the competing effects of surface and dipolar interaction on the susceptibility. The curves are obtained for $\tilde{\xi} = 0.008$ and small (and increasing) surface anisotropy parameter ζ . These results show that the surface anisotropy, in the present case of positive ζ , has the opposite effect to that of DDI. More precisely, this implies that surface effects can screen out the effect of DDI and the other way round. This confirms the results of Ref. 2 for equilibrium properties for both negative and positive ζ .

E. Discussion

Very often the experimental results related with the dynamics of an assembly of DDI-coupled nanoparticles are analyzed with the help of the Vogel-Fulcher law^{38,46,48,50–52}

$$\Gamma = \tau_0^{-1} e^{\frac{\Delta E}{k_B(T - \theta_{VF})}} \quad (29)$$

where $\nu_0 = \tau_0^{-1} \simeq 10^9 - 10^{12}$ Hz, θ_{VF} represents an effective temperature supposed to include the DDI correction and ΔE is the energy barrier, which reads $\Delta E = K_2 V$ in the case of uniaxial anisotropy and zero field. The main concern with this phenomenological formula is to provide an interpretation of the parameter θ_{VF} on physical grounds. Accordingly, in Ref. 50. there is a discussion of a few approaches in this regard. For instance, it is shown how the work of Shtrikman and Wohlfarth⁵³ leads to an expression of θ_{VF} in terms of the applied magnetic field and how the work by Déjardin³⁸ yields an expression in terms of the DDI coupling. In the work of Landi itself θ_{VF} is expressed in terms of the inter-particle distance and other parameters such as the particles magnetic moment and the uniaxial-anisotropy energy.

Here we show that our formalism is in full agreement with the previous results and further extends them along the following lines: i) surface anisotropy, ii) particles spatial distribution and shape of the assembly, iii) damping parameter.

In Eq. (24) the factor $\Gamma_0(h, \sigma, \zeta, \lambda)$ depends on the applied field, surface anisotropy and damping, together with other parameters, as is seen in Eq. (22). It turns out that in fact the prefactor $\Gamma_p^+(h, \sigma, \zeta, \lambda)$ is a slowly varying function of ζ and as such can be written as $\Gamma_p^+(h, \sigma, \zeta, \lambda) \simeq \tilde{\Gamma}(h, \sigma, \lambda)$. This implies that the dependence of the relaxation rate $\Gamma_0(h, \sigma, \zeta, \lambda)$ ζ is mainly borne by the energy barrier $\Delta\mathcal{E}_+^{(0)}(\zeta)$. Therefore, in zero field $\Delta\mathcal{E}_+^{(0)}(\zeta) \simeq -\sigma + \sigma\zeta/4$ and upon expanding in ζ we obtain

$$\Gamma(h, \sigma, \zeta, \lambda, \xi) \simeq \tilde{\Gamma}(h=0, \sigma, \lambda) e^{\sigma} \left(1 + \frac{\sigma\zeta}{4} + \frac{\xi^2}{6} \mathcal{S} \right) \quad (30)$$

where $\mathcal{S}(\lambda)$ is defined in Eq. (25). Note that $\tilde{\Gamma}(h=0, \sigma, \lambda)$ is given in the second line of Eq. (6) in Ref. 37.

Now, an expansion of Eq. (29) with respect to θ_{VF}/T yields⁵⁰

$$\Gamma = \tau_0^{-1} e^{\frac{\Delta E}{k_B(T-\theta_{VF})}} \simeq \tau_0^{-1} e^{\sigma} \left(1 + \sigma \frac{\theta_{VF}}{T} \right)$$

which is of the same form as our expression (30). Next, using Néel's approximation with a constant prefactor τ_0^{-1} , thus ignoring any dependence on temperature, damping and applied field, $\tilde{\Gamma}(h=0, \sigma, \lambda)$ can be identified with τ_0^{-1} . Then, we can further identify the terms between parentheses leading to the following expression for θ_{VF} (in Néel's approximation)

$$\frac{\theta_{VF}}{T} = \frac{\zeta}{4} + \frac{1}{6\sigma} (\xi^2 \mathcal{S}). \quad (31)$$

This expression provides a somewhat “microscopic” description of the phenomenological parameter θ_{VF} in terms of the inter-particle interactions, the surface anisotropy and damping. Indeed, the last term in (31), which is similar to the one derived in Ref. 50, includes both the damping parameter and the shape of the assembly, owing to the expression of $\mathcal{S}(\lambda)$ [see Eq. (25)]. In addition, we note that ξ is proportional to the assembly concentration² C_V and thereby to a^{-3} , a being the inter-particle distance. Therefore, we expect that in the absence of surface anisotropy, θ_{VF} scales as $\theta_{VF} \sim C_V^2 \sim a^{-6}$. In Ref. 46 experimental estimates of θ_{VF} are given for an assembly of Ni nanoparticles with varying concentration. A comparison of Eq. (31) with the corresponding data is given in Fig. 6.

On the other hand, the first term in Eq. (31) accounts for the contribution from surface anisotropy. As discussed earlier, in practice it should be possible to adjust the assembly characteristics (assembly shape, particles size and underlying material) so as to achieve to some extent a compensation between surface effects and the DDI contribution. This could in principle suppress the dependence of θ_{VF} on the assembly concentration. In addition, the term in ζ can also be used to extract from the experimental data an estimate of the surface anisotropy coefficient ζ by reading off the intercept from the plot in Fig. 6.

In the most often encountered situation where the particles anisotropy is modeled with an effective uniaxial anisotropy of constant K_{eff} , as would apply for elongated particles, dropping the ζ term, the effective temperature θ_{VF} explicitly reads (as a function of the assembly con-

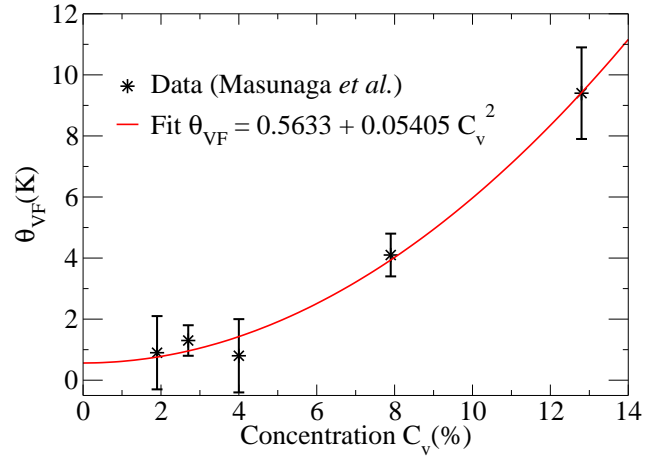


Figure 6: θ_{VF} against the assembly concentration. (stars) Experimental data from Masunaga *et al.*⁴⁶ and (full line) fit of Eq. (31).

centration C_V)

$$k_B \theta_{VF} = \left(\frac{\mu_0}{4\pi} \right)^2 \frac{(M_s^2 V)^2}{K_{\text{eff}} V} \frac{\mathcal{S}}{6} \times C_V^2. \quad (32)$$

For example, consider a monodisperse assembly of spherical cobalt nanoparticles of 3 nm in diameter with $M_s \simeq 1.4 \times 10^6 \text{ J.T}^{-1}.\text{m}^{-3}$, $K_{\text{eff}} \simeq 5 \times 10^5 \text{ J.m}^{-3}$, and $C_V \simeq 1\%$. Then, if the assembly is assumed to be in the form of a box-shaped sample with its particles arranged into a simple cubic lattice, the lattice sums \mathcal{R} and \mathcal{T} were given earlier in the thermodynamic limit. Then, using $F(\lambda) \simeq 1$ and $S_2 \simeq 1$, the factor \mathcal{S} evaluates to $\mathcal{S} \simeq 45$. This yields $\theta_{VF} \simeq 0.05 \text{ K}$, which is small compared to the particle's blocking temperature $T_B \simeq 14 \text{ K}$. However, one should keep in mind that θ_{VF} scales with the particle's volume.

It is worth emphasizing the fact that θ_{VF} given by Eq. (32) is independent of temperature, as can be often encountered in the literature. However, if we take account of surface anisotropy, Eq. (31) shows that the phenomenological parameter θ_{VF} is in fact a linear function of temperature via the term in ζ . This can be understood by noting that surface anisotropy, which is of cubic nature in the EOPS model, drastically modifies the energy potential and thereby affects the dynamics of the particle's magnetization. As a consequence, the effect of DDI becomes strongly dependent on the thermal fluctuations and the elementary switching processes they induce.

V. CONCLUSION

We have studied the combined effects of surface anisotropy and dipolar inter-cluster interactions on the dynamic response of a mono-disperse assembly of magnetic nanoclusters with textured anisotropy. We have derived semi-analytical expressions for the in-phase and

out-of-phase components of the AC susceptibility as functions of temperature, applied field, surface anisotropy, damping, frequency, and (weak) dipolar interactions. If we ignore the surface anisotropy, we recover the well known results of frequency- and interaction-induced shift in both the maximum of χ' and χ'' and of the temperature T_{\max} thereat, taking into account the effect of the assembly shape (oblate or prolate). In the presence of surface anisotropy we have derived and used a semi-analytical expression for the relaxation time and investigated the effect of surface (cubic) anisotropy. We have done so in the limit of small field, high uniaxial anisotropy barrier and weak surface anisotropy. The expressions obtained for the small ζ show that the relaxation rate or the switching probability increases with surface anisotropy, but the equilibrium susceptibility decreases, thus leading to an overall upward shift of T_{\max} . When the inter-particle interactions are switched on, a competition sets in between the latter and surface anisotropy that may

lead, in adequately prepared samples, to a mutual compensation of the two effects.

Finally, our results for the relaxation rate have been analyzed in connection with the so-called Vogel-Fulcher law and an expression for the *ad hoc* effective temperature has been given in terms of the inter-particle dipolar interactions, the intra-particle surface anisotropy and the damping parameter, in addition to the other physical parameters such as the applied magnetic field and uniaxial anisotropy.

Acknowledgments

F.V. and H.K. would like to thank Denis Ledue for discussions and useful comments in the early stage of this work.

-
- * Electronic address: francois.vernay@univ-perp.fr
† Electronic address: hamid.kachkachi@univ-perp.fr
- ¹ G. Margaritis, K.N. Trohidou, and H. Kachkachi, Phys. Rev. B **85**, 024419 (2012).
 - ² Z. Sabsabi, F. Vernay, O. Iglesias, H. Kachkachi, Phys. Rev. B **88**, 104424 (2013).
 - ³ D. A. Garanin and H. Kachkachi, Phys. Rev. Lett. **90**, 065504 (2003).
 - ⁴ H. Kachkachi and E. Bonet, Phys. Rev. B **73**, 224402 (2006).
 - ⁵ H. Kachkachi, J. Magn. Magn. Mater. **316**, 248 (2007).
 - ⁶ R. Yanes, O. Chubykalo-Fesenko, H. Kachkachi, D. A. Garanin, R. Evans, and R. W. Chantrell, Phys. Rev. B **76**, 064416 (2007).
 - ⁷ J.I. Gittleman, B. Abeles, and S. Bozowski, Phys. Rev. B **9**, 3891 (1974).
 - ⁸ J.-L. Dormann, D. Fiorani, and E. Tronc, Adv. Chem. Phys. **98**, 283 (1997).
 - ⁹ F. Luis, F. Petroff, and J. Bartolomé, J. Phys.: Condens. Mat. **16**, 5109 (2004).
 - ¹⁰ E. Tronc et al., J. Magn. Magn. Mater. **262**, 6 (2003).
 - ¹¹ P.E. Jönsson and J.L. Garcia-Palacios, Europhys. Lett. **55**, 418 (2001).
 - ¹² D. V. Berkov and N. L. Gorn, J. Phys.: Condens. Matter **13**, 9369 (2001).
 - ¹³ Yu. Raikher and M.I. Shliomis, Adv. Chem. Phys. **87**, 595 (1994).
 - ¹⁴ P. Svedlindh, T. Jonsson, J. L. Garcia-Palacios, Journal of Magnetism and Magnetic Materials **169**, 323 (1997).
 - ¹⁵ Y. L. Raikher and V. I. Stepanov, Phys. Rev. B **55**, 15005 (1997).
 - ¹⁶ J.-O. Andersson, C. Djurberg, T. Jonsson, P. Svedlindh, and P. Nordblad, Phys. Rev. B **56**, 13983 (1997).
 - ¹⁷ J. L. Garcia-Palacios and F. J. Lazaro, Phys. Rev. B **58**, 14937 (1998).
 - ¹⁸ L. Spinu, *Etudes des propriétés dynamiques d'assemblées de nanoparticule magnétiques* (Ph.D. thesis, Université Paris-Sud, Orsay, 1998).
 - ¹⁹ J. L. Dormann, D. Fiorani, R. Cherkou, E. Tronc, F. Lucari, F. D'Orazio, L. Spinu, M. Noguès, H. Kachkachi and J. P. Jolivet, J. Magn. Magn. Mater. **203**, 23 (1999).
 - ²⁰ P. E. Jönsson, S. Felton, P. Svedlindh, P. Nordblad, and M. F. Hansen, Phys. Rev. B **64**, 212402 (2001).
 - ²¹ Y. L. Raikher and V. I. Stepanov, Phys. Rev. B **66**, 214406 (2002).
 - ²² E. Tronc, D. Fiorani, M. Noguès, A.M. Testa, F. Lucari, F. D'Orazio, J. M. Grenèche, W. Wernsdorfer, N. Galvez, C. Chanéac, D. Mailly, and J. P. Jolivet, J. Magn. Magn. Mater. **262**, 6 (2003).
 - ²³ D. Brinis, A. Laggoun, D. Ledue, R. Patte, J. Appl. Phys. **115**, 173906 (2014).
 - ²⁴ H. Kachkachi and D. S. Schmool, Eur. Phys. J. B **56**, 27 (2007).
 - ²⁵ P.E. Jönsson and J.L. Garcia-Palacios, Phys. Rev. B **64**, 174416 (2001).
 - ²⁶ J.L. Garcia-Palacios, Adv. Chem. Phys. **112**, 1 (2000).
 - ²⁷ M.I. Shliomis and V.I. Stepanov, J. Magn. Magn. Mater. **122**, 176 (1993).
 - ²⁸ D.A. Garanin, E.C. Kennedy, D.S.F. Crothers, and W.T. Coffey, Phys. Rev. E **60**, 6499 (1999).
 - ²⁹ A. Aharoni, Phys. Rev. **177**, 793 (1969).
 - ³⁰ J.S. Langer, Phys. Rev. Lett. **21**, 973 (1968).
 - ³¹ J.S. Langer, Ann. Phys. (N.Y.) **54**, 258 (1969).
 - ³² H.B. Braun, J. Appl. Phys. **76**, 6310 (1994).
 - ³³ H.B. Braun, Phys. Rev. B **50**, 16501 (1994).
 - ³⁴ H. Kachkachi, Eur. Phys. Lett. **62**, 650 (2003).
 - ³⁵ H. Kachkachi, J. Mol. Liquids **114**, 113 (2004).
 - ³⁶ S.V. Titov, H. Kachkachi, Y.P. Kalmykov, W.T. Coffey, Phys. Rev. B **72**, 134425 (2005).
 - ³⁷ P.-M. Déjardin, H. Kachkachi, Yu. Kalmykov, J. Phys. D **41**, 134004 (2008).
 - ³⁸ P.-M. Déjardin, J. App. Phys. **110**, 113921 (2011).
 - ³⁹ J. L. Dormann, F. D'Orazio, F. Lucari, E. Tronc, P. Prené, J. P. Jolivet, D. Fiorani, R. Cherkou, and M. Noguès, Phys. Rev. B **53**, 14291 (1996).
 - ⁴⁰ H. Mamiya and I. Nakatani, J. Magn. Magn. Mater. **177**, 966 (1998).
 - ⁴¹ J.L. Garcia-Palacios and D.A. Garanin, Phys. Rev. B **70**,

- 064415 (2004).
- ⁴² H. Shim, A. Manivannan, M. Seehra, K. M. Reddy, and A. Punnoose, *J. Appl. Phys* **99**, 08Q503 (2006).
- ⁴³ V. Singh, M. S. Seehra, and J. Bonevich, *J. Appl. Phys* **99**, 07B518 (2009).
- ⁴⁴ V. Singh, M. S. Seehra, and J. Bonevich, *J. Appl. Phys* **103**, 07D524 (2009).
- ⁴⁵ J. F. Godsell, T. Bala, K. M. Ryan, and S. Roy, *J. Appl. Phys. D: Applied Physics* **44**, 32 (2011).
- ⁴⁶ S. H. Masunaga, R. F. Jardim, P. F. P. Fichtner, and J. Rivas, *Phys. Rev. B* **80**, 184428 (2009).
- ⁴⁷ D. Ledue and R. Patte and H. Kachkachi, *J. Nanoscience and Nanotechnology* **12**, 4953 (2012).
- ⁴⁸ J. S. Lee, R. P. Tan, J. H. Wu, and Y. K. Kim, *Appl. Phys. Lett.* **99**, 062506 (2011).
- ⁴⁹ V. Russier, C. de Montferrand, Y. Lalatonne, and L. Motte, *J. Appl. Phys.* **112**, 073926 (2012).
- ⁵⁰ G. Landi, *J. Appl. Phys.* **113**, 163908 (2013).
- ⁵¹ D. Fiorani, *J. Phys.: Conf. Series* **521**, 012006 (2014).
- ⁵² P. Allia, *J. Phys.: Conf. Series* **521**, 012008 (2014).
- ⁵³ S. Shtrikman and E. Wohlfarth, *Phys. Lett. A* **85**, 467 (1981).